

NLO PDFs from the ABMP16 fit

S. Alekhin^{a,b}, J. Blümlein^c, and S. Moch^a

^a *II. Institut für Theoretische Physik, Universität Hamburg
Luruper Chaussee 149, D-22761 Hamburg, Germany*

^b *Institute for High Energy Physics
142281 Protvino, Moscow region, Russia*

^c *Deutsches Elektronensynchrotron DESY
Platanenallee 6, D-15738 Zeuthen, Germany*

Abstract

We perform a global fit of parton distribution functions (PDFs) together with the strong coupling constant α_s and the quark masses m_c , m_b and m_t at next-to-leading order (NLO) in QCD. The analysis applies the $\overline{\text{MS}}$ renormalization scheme for α_s and all quark masses. It is performed in the fixed-flavor number scheme for $n_f = 3, 4, 5$ and uses the same data as the previous fit of the ABMP16 PDF at next-to-next-to-leading order (NNLO). The new NLO PDFs complement the set of ABMP16 PDFs and are to be used consistently with NLO QCD predictions for hard scattering processes. At NLO we obtain the value $\alpha_s^{(n_f=5)}(M_Z) = 0.1191 \pm 0.0011$ compared to $\alpha_s^{(n_f=5)}(M_Z) = 0.1147 \pm 0.0008$ at NNLO.

Parton distribution functions (PDFs) are an indispensable ingredient in theory predictions for hadronic scattering processes within perturbative QCD. Currently, the state-of-art calculations for many standard-candle processes at the Large Hadron Collider (LHC) and elsewhere are based on the QCD corrections up to the next-to-next-to-leading order (NNLO) in the strong coupling constant α_s [1]. In order to match this theoretical accuracy the PDFs and other input parameters such as α_s and the quark masses m_c , m_b and m_t also have to be determined at the same order of perturbation theory, that is with account of the NNLO QCD corrections. In many instances, however, the Wilson coefficient functions or hard partonic scattering cross sections are known to the next-to-leading order (NLO) only. This concerns in particular Monte-Carlo studies at the LHC. Then, to meet the consistency requirements, NLO PDFs and the respective NLO values for α_s and the heavy-quark masses are to be used. The NLO fit of PDFs is therefore of immediate practical use and also provides a very good consistency check of the perturbative stability of QCD calculations.

In this article we describe the NLO version of the recent ABMP16 PDF fit, i.e., the NLO analysis, which applies the $\overline{\text{MS}}$ scheme for α_s and all heavy-quark masses. It uses the same data, their uncertainty treatment and the general theoretical framework, e.g., the fixed-flavor number scheme for $n_f = 3, 4$ and 5 , as in the previous fit of the ABMP16 PDF at NNLO. The only difference resides in the order of the perturbative corrections to the QCD evolution equations and for the Wilson coefficients, which are now limited to NLO accuracy. Due to the obvious correlations of the various parameters in the PDFs with the value of α_s and those of the quark masses m_c , m_b and m_t , all quantities are extracted simultaneously from the global fit following our previous analyses [2–4]. The article discusses in detail the differences in their determinations at NLO and NNLO accuracy. Specific attention is paid to the treatment of power corrections in the description of deep-inelastic scattering (DIS) data, i.e. higher-twist effects which are relevant beyond the leading twist collinear factorization approximation. The final fit results are made available as data grids for use with the LHAPDF library (version 6) [5] and the features of the various grids are briefly discussed.

The values of χ^2 obtained in the present analysis for various data sets are listed in Tab. I in comparison with the earlier ones for the NNLO ABMP16 fit. The overall quality of the data description does not change dramatically between the NLO and the NNLO versions, where the former features a somewhat bigger total value of χ^2 . Of course, the theoretical description at NNLO accuracy comes with a significantly reduced theoretical uncertainty due to variations of the factorization and renormalization scales compared to the NLO one. Nevertheless, for specific scattering reactions the NNLO corrections are crucial for the respective data sets. This holds in particular for the c -quark and, to a lesser extent, for b -quark production in DIS and for hadronic t -quark pair-production, which constrain the heavy-quark masses and which are fitted together with α_s simultaneously with the PDFs. The theoretical description at NNLO accuracy is also essential for the parameters of the higher (dynamical) twist, which contribute additively to the leading twist. The x -dependent twist-four contributions to the longitudinal and transverse DIS cross sections have been determined in the NNLO version (cf. Tab. VIII in Ref. [4]) and their central values are kept fixed in the present analysis. Also other fitted parameters like the data set normalizations are taken over unchanged from the NNLO analysis (cf. Tab. I in Ref. [4]). This provides a better consistency between the PDF sets obtained with different theoretical accuracy. At the same time the uncertainties in the normalization and higher twist parameters are computed in the same way as in the NNLO fit [4], by propagation of the ones in experimental data and simultaneously with other fit parameters in order to take into account their correlations and, therefore, provide a consistent uncertainty treatment in the NLO and NNLO fits. Therefore, the uncertainties obtained for the

Experiment	Process	NDP	χ^2	
			NLO	NNLO
DIS				
HERA I+II	$e^\pm p \rightarrow e^\pm X$	1168	1528	1510
	$e^\pm p \rightarrow \overset{(-)}{\nu} X$			
Fixed-target (BCDMS, NMC, SLAC)	$l^\pm p \rightarrow l^\pm X$	1008	1176	1145
DIS heavy-quark production				
HERA I+II	$e^\pm p \rightarrow e^\pm c X$	52	58	66 ^a
H1, ZEUS	$e^\pm p \rightarrow e^\pm b X$	29	21	21
Fixed-target (CCFR, CHORUS, NOMAD, NuTeV)	$\overset{(-)}{\nu} N \rightarrow \mu^\pm c X$	232	173	178
DY				
ATLAS, CMS, LHCb	$pp \rightarrow W^\pm X$	172	229	223
	$pp \rightarrow ZX$			
Fixed-target (FNAL-605, FNAL-866)	$pN \rightarrow \mu^+ \mu^- X$	158	219	218
Top-quark production				
ATLAS, CMS	$pp \rightarrow tqX$	10	5.7	2.3
CDF&DØ	$\bar{p}p \rightarrow tbX$	2	1.9	1.1
	$\bar{p}p \rightarrow tqX$			
ATLAS, CMS	$pp \rightarrow t\bar{t}X$	23	14	13
CDF&DØ	$\bar{p}p \rightarrow t\bar{t}X$	1	1.4	0.2
Total		2855	3427	3378

^aThis value corrects a misprint in Table V of Ref. [4].

TABLE I: The values of χ^2 obtained in the present analysis at NLO for the data on inclusive DIS, the DY process, and on heavy-quark production in comparison with the ones of the ABMP16 fit at NNLO [4].

data normalization and the twist-four contributions at NLO are only marginally different from those reported at NNLO in Tabs. I and VIII in Ref. [4].

Closer inspection of the χ^2 -values in Tab. I reveals the largest differences between NLO and NNLO for the fixed-target DIS data, which can be explained by the kinematic coverage of this data sample, which is predominantly in the low- Q^2 region. For the Drell-Yan (DY) data the impact of the NNLO QCD corrections is less pronounced and the corresponding improvement in the value of χ^2 is small. For the heavy-quark production data on the other hand the trend is not uniform, i.e., for some data sets the χ^2 -values at NLO are larger and vice versa for others. In this context it is worth noting, that to a certain extent the impact of missing NNLO terms in the NLO fit is compensated by tuning the values of heavy-quark masses.

The ABMP16 PDF sets at NLO and NNLO are compared in Fig. 1 for the case of $n_f = 3$ flavors at the scale $\mu = 3$ GeV. Both sets are based on the same flexible parametrization used in

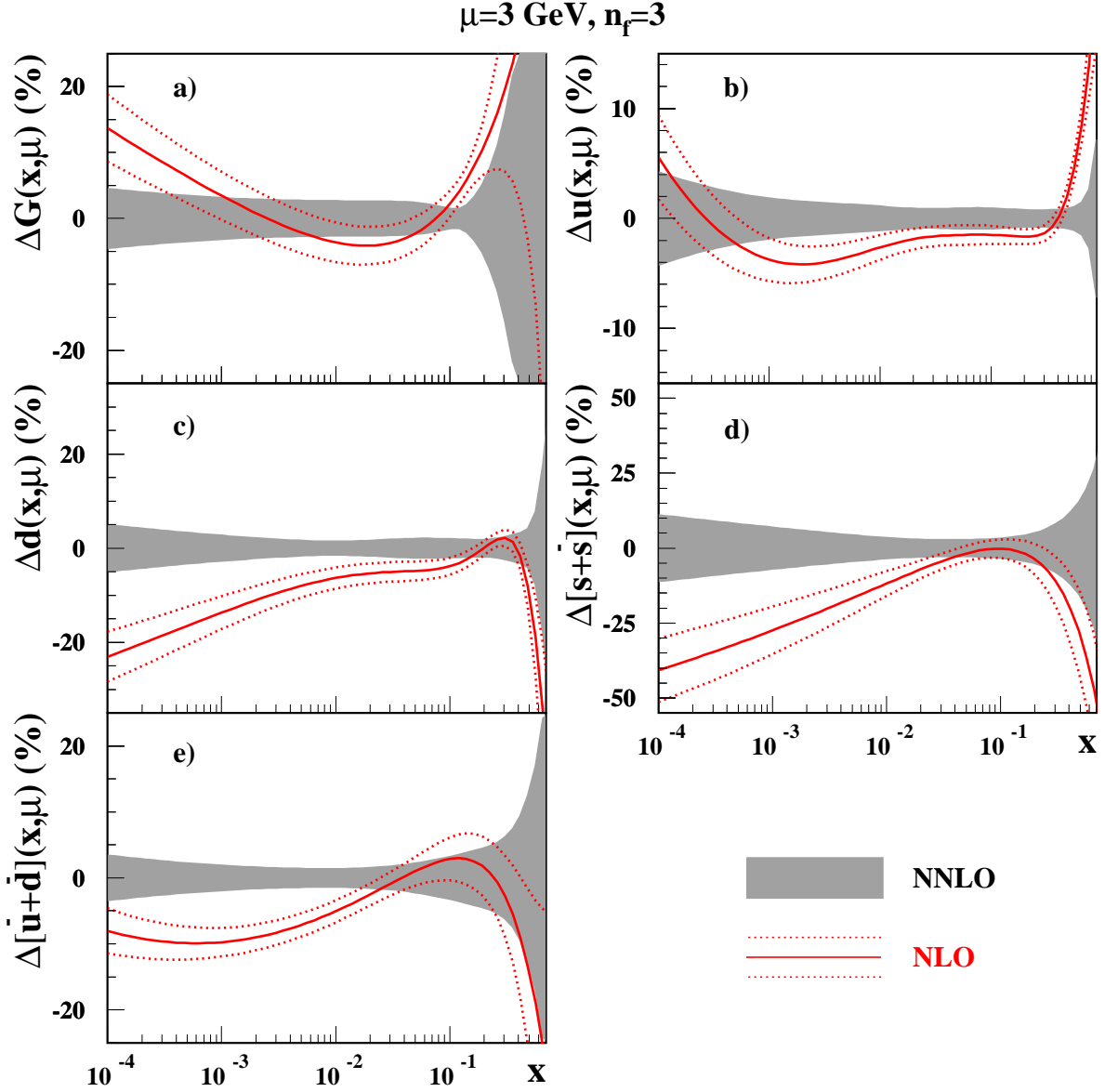


FIG. 1: The 1σ band for the $n_f = 3$ flavor NNLO ABM16 PDFs [4] for **a)** gluon, **b)** up-quarks **c)** down-quarks **d)** the symmetrized strange sea and **e)** the non-strange sea, at the scale of $\mu = 3 \text{ GeV}$ versus x (shaded area) compared with the relative difference of those PDFs to the NLO ABMP16 ones obtained in the present analysis (solid lines). The dotted lines display 1σ band for the NLO PDFs.

Ref. [4]. For the gluon PDF, we see in Fig. 1a that the NLO PDFs are larger by about 15% in the small- x and the large- x region, i.e., for $x \lesssim 10^{-4}$ and $x \gtrsim 0.3$, respectively. In these kinematic regions for example the DIS coefficient functions receive systematically large corrections at higher orders, which need to be compensated by the gluon PDF if the fit is performed at NLO accuracy. The u -quark PDF in Fig. 1b does not show any big changes, except for large $x \gtrsim 0.6$, while the d -quark PDF Fig. 1c at NLO is smaller in the entire range $x \lesssim 10^{-1}$ and decreasing more than 20% for $x \lesssim 10^{-4}$. A similar observation holds for the strange sea displayed in Fig. 1d, which is smaller by even 50% for $x \lesssim 10^{-4}$ at NLO, however, the PDF uncertainties for this quantity are correspondingly larger. On the other hand, the non-strange sea in Fig. 1e does not show big

relative differences between NLO and NNLO. There is only a slight decrease of the NLO result by 5% to 10% for $x \lesssim 10^{-2}$. The small- x sea iso-spin asymmetry $\bar{d} - \bar{u}$ at NLO goes lower than the NNLO one, as can be seen from a comparison of Figs. 1b) and 1c). This reflects the impact of the NNLO corrections on the data for Drell-Yan production, which drive this asymmetry in our fit.

fit ansatz		$\alpha_s(M_Z)$	
higher twist modeling	cuts on DIS data	NLO	NNLO
higher twist fitted	$Q^2 > 2.5 \text{ GeV}^2, W > 1.8 \text{ GeV}$	0.1191(11)	0.1147(8)
higher twist fixed at 0	$Q^2 > 10 \text{ GeV}^2, W^2 > 12.5 \text{ GeV}^2$	0.1212(9)	0.1153(8)
	$Q^2 > 15 \text{ GeV}^2, W^2 > 12.5 \text{ GeV}^2$	0.1201(11)	0.1141(10)
	$Q^2 > 25 \text{ GeV}^2, W^2 > 12.5 \text{ GeV}^2$	0.1208(13)	0.1138(11)

TABLE II: The values of $\alpha_s(M_Z)$ obtained in the NLO and NNLO variants of the ABMP16 fit with various kinematic cuts on the DIS data imposed and different modeling of the higher twist terms.

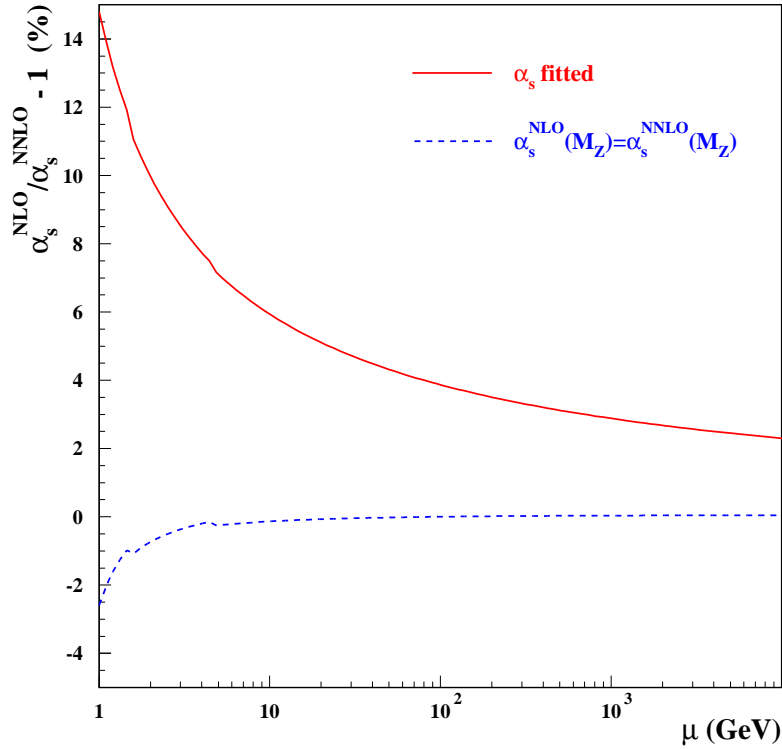


FIG. 2: The relative difference between $\alpha_s^{\text{NLO}}(\mu)$ and $\alpha_s^{\text{NNLO}}(\mu)$ as a function of the renormalization scale μ . The solid line denotes the results of the present analysis (NLO) and of Ref. [4] (NNLO), the dashed line displays the ones derived using matching $\alpha_s^{\text{NLO}} = \alpha_s^{\text{NNLO}}$ at the scale M_Z .

The value of $\alpha_s(M_Z)$ at the scale of Z-boson mass M_Z obtained in the present analysis at NLO is larger than the one obtained in the NNLO variant of ABMP16 fit [4], the relative difference amounting to about 4%, which is well comparable to the estimated margin due to variations of the

factorization and renormalization scales, cf. Ref. [6]. In the scheme with $n_f = 5$ light flavors we find

$$\begin{aligned}\alpha_s^{\text{NLO}}(M_Z) &= 0.1191 \pm 0.0011, \\ \alpha_s^{\text{NNLO}}(M_Z) &= 0.1147 \pm 0.0008,\end{aligned}\tag{1}$$

as listed in the first line of Tab. II together with the kinematic cuts imposed on the DIS data. The description of DIS data at those low values of Q^2 and W for the invariant mass of the hadronic system, where $W^2 = M_p^2 + Q^2(1-x)/x$ with the proton mass M_p , requires modeling of the higher-twist terms. This has been discussed extensively in the ABMP16 analyses at NNLO [4]. Following the theoretical framework there, the fitted twist-four contributions to the longitudinal and transverse DIS cross sections have been used to determine the value of $\alpha_s^{\text{NLO}}(M_Z)$ in Eq. (1). Alternatively, one can impose cuts both on Q^2 and W^2 to eliminate data from the kinematic regions most sensitive to the higher-twist terms. Then, the fit can be performed with all higher-twist terms set to zero and the results are shown in Tab. II. These variants of the fit with substantially higher cuts on Q^2 and W^2 and higher-twist terms set to zero display very good stability of the value of $\alpha_s(M_Z)$, both at NLO and NNLO, and therefore very good consistency of the chosen approach.

Finally, in one of the variants of present analysis we impose the low cuts on Q^2 and W^2 from the first line of Tab. II, while fitting also the twist-four contributions. This gives an improvement in the value of χ^2 equal to 86 and $\alpha_s^{\text{NLO}}(M_Z) = 0.1227 \pm 0.0011$, which is a slightly larger value than those quoted in Tab. II for the fits with higher cuts on Q^2 and W^2 . The magnitude of these shifts in $\alpha_s(M_Z)$ may also be considered as an indication for the limitations of the NLO approximation.

Nevertheless, the observed difference between $\alpha_s^{\text{NLO}}(\mu)$ and $\alpha_s^{\text{NNLO}}(\mu)$ is quite essential, particularly at small scales μ , where the NLO and NNLO results differ by more than 10%, as illustrated in Fig. 2 for a wide range of scales. This difference is to a great extent responsible for the perturbative stability of QCD calculations at the hard scales currently probed in scattering processes at colliders. Asymptotic freedom in QCD, i.e. stability of theoretical predictions under higher order perturbative corrections requires very large scales. On the other hand, for realistic kinematics including experiments at the LHC a consistent setting of $\alpha_s(M_Z)$ is very important to achieve sensible theoretical predictions.¹

In this context it is worth to mention the conventional choice $\alpha_s^{\text{NLO}}(M_Z) = \alpha_s^{\text{NNLO}}(M_Z)$, which is adopted as a part of PDF4LHC recommendations [9] and employed in the CT14 [10] and NNPDF [11] PDF fits. Under this assumption the value of α_s obtained at NLO is very close to the NNLO one in a wide range of scales, as shown in Fig. 2. As a result, such an approach has significant limitations when studying the convergence of the perturbative expansion, since the NLO predictions obtained with these PDF sets might be very similar to the NNLO ones simply due to the convention used.

The values for the heavy-quark masses obtained in the NLO and NNLO variants of the ABMP16 analysis are given in Tab. III. The comparison of the difference between these values indicates again the limitations of the NLO approximation. The shifts are more essential for m_c and m_t , since the NNLO corrections are absolutely essential in order to achieve a good description of the data on DIS c -quark production and t -quark hadro-production. On the other hand, the data

¹ Recent reviews on determinations of $\alpha_s(M_Z)$, particularly those involving PDF fits, can be found in [7], in Sec. 4 of Ref. [1] and in Sec. III.D of Ref. [4]. Determinations of $\alpha_s(M_Z)$ in DIS and including jet cross section measurements have been discussed in Ref. [8].

on DIS b -quark production are less precise, therefore the value of m_b extracted from the fit suffers from the larger uncertainties and is less sensitive to the impact of the NNLO corrections, cf. Tab. III.

	NLO	NNLO
$m_c(m_c)$ [GeV]	1.175 ± 0.033	1.252 ± 0.018
$m_b(m_b)$ [GeV]	3.88 ± 0.13	3.84 ± 0.12
$m_t(m_t)$ [GeV]	162.1 ± 1.0	160.9 ± 1.1

TABLE III: The values of the c -, b - and t -quark masses in the $\overline{\text{MS}}$ scheme in units of GeV obtained in the NLO and NNLO variants of the ABMP16 fit. The quoted errors reflect the uncertainties in the analyzed data.

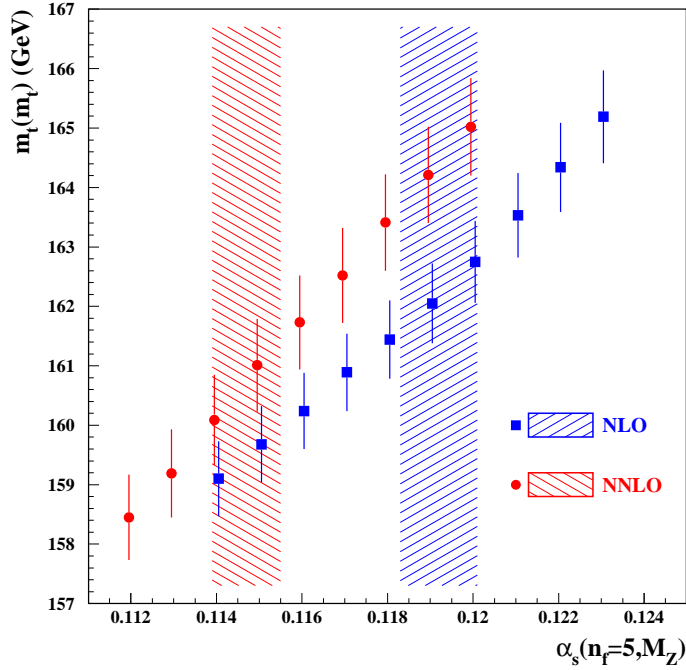


FIG. 3: The $\overline{\text{MS}}$ values of the t -quark mass $m_t(m_t)$ obtained in the variants of the NLO ABMP16 fit with $\alpha_s^{(n_f=5)}(M_Z)$ fixed (squares) in comparison to ones at NNLO (circles). The left-tilted and right-tilted hatch represent the 1σ bands for $\alpha_s^{(n_f=5)}(M_Z)$ obtained in the ABMP16 nominal fits at NLO and NNLO, respectively. The points are slightly shifted left and right to prevent overlapping.

In addition, the value of m_t demonstrates strong correlation with the value of α_s , since the Born cross section for $t\bar{t}$ -production is proportional to α_s^2 , so that changes in the value of α_s induce shifts in fitted value of m_t [3, 4]. This is quantified in Fig. 3, where the values of m_t determined in variants of the present analysis with fixed values of α_s demonstrate a nearly linear dependence on α_s . It is interesting to note, though, that at NLO this dependence is somewhat shallower than for the similar fit at NNLO since due to important missing QCD corrections of $O(\alpha_s^4)$ in the hadronic $t\bar{t}$ -production cross section at NLO, $\sigma(t\bar{t})$ is less sensitive to the α_s variations at this order. For the same reason the NLO value of m_t is substantially larger than the NNLO one. This comparison

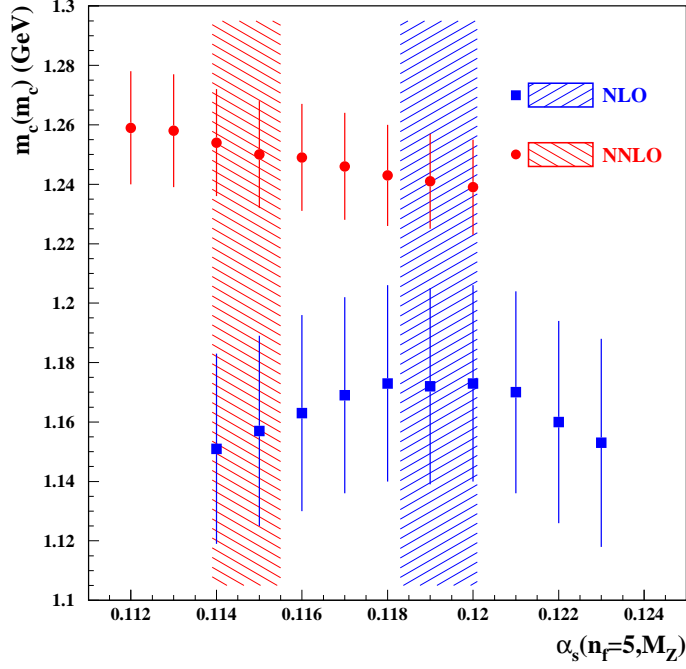


FIG. 4: The same as in Fig. 3 for the $\overline{\text{MS}}$ value of the c -quark mass $m_c(m_c)$.

demonstrates the necessity for a consistent treatment of the higher order corrections to the hard partonic scattering together with the parameter choices for α_s and m_t , especially in analysis of the $t\bar{t}$ -production data. To that end, the PDFs from the variants entering Fig. 3 with the a fixed value of $\alpha_s(M_Z)$ in the range of $0.114 \div 0.123$ are made available as well. It should be stressed, though, that those PDFs at preselected values of $\alpha_s(M_Z)$ are not providing the χ^2 minimum in analysis of all the data.

In contrast, the determination of the charm-quark mass m_c is not very sensitive to the value of α_s because the variation of α_s is compensated by a change in the gluon distribution at small x [12] (cf. also Tab. B in Ref. [4] for correlations between α_s and the quark masses). Indeed, the fitted value of m_c only changes by ± 20 MeV for a variation of α_s in a wide range, cf. Fig. 4. However, the NNLO corrections to the Wilson coefficients for DIS heavy-quark production still have significant impact on m_c , moving it up by ~ 100 MeV and reducing its uncertainty. The relatively weak correlation of m_c with α_s in Fig. 4 is in contrast to the observed behavior in the MMHT14 PDF set [13], where the particular variable flavor number scheme applied causes a linear relation between m_c and α_s in those fits and the charm-quark mass has been treated as a variable parameter and the resulting values of χ^2 when fitting data on DIS c -quark production have been quantified. See Sec. 3.2 and Tabs. 4 and 5 in Ref. [1] for a review of the theoretical treatments of DIS c -quark production used in PDF fits and Tab. 2 in Ref. [13] as well as Tab. 12 in Ref. [1] for the respective values of m_c , α_s and χ^2 in the MMHT14 PDF set.

The grids for the NLO PDFs obtained in the present analysis are accessible with the LHAPDF library (version 6) [5] and available for download under <http://projects.hepforge.org/lhapdf>. For a fixed number of flavors, $n_f = 3, 4$ and 5, we provide

ABMP16_3_nlo (0+29),

PDF set	$\alpha_s^{(n_f=5)}(M_Z)$	$m_c(m_c)$ [GeV]	$m_b(m_b)$ [GeV]	m_b^{pole} [GeV]	$m_t(m_t)$ [GeV]	m_t^{pole} [GeV]
0	0.11905	1.175	3.880	4.488	162.08	171.44
1	0.11905	1.175	3.880	4.488	162.08	171.44
2	0.11906	1.175	3.880	4.489	162.08	171.44
3	0.11905	1.175	3.880	4.488	162.08	171.44
4	0.11899	1.175	3.880	4.488	162.08	171.43
5	0.11898	1.175	3.880	4.487	162.08	171.43
6	0.11907	1.175	3.880	4.489	162.08	171.44
7	0.11906	1.175	3.880	4.489	162.08	171.44
8	0.11911	1.175	3.880	4.489	162.08	171.44
9	0.11858	1.175	3.880	4.482	162.08	171.40
10	0.11925	1.175	3.880	4.491	162.08	171.46
11	0.11914	1.175	3.880	4.490	162.08	171.45
12	0.11910	1.176	3.880	4.489	162.08	171.44
13	0.11904	1.173	3.880	4.488	162.08	171.44
14	0.11909	1.203	3.880	4.489	162.08	171.44
15	0.11912	1.170	3.880	4.489	162.08	171.44
16	0.11930	1.169	3.877	4.489	162.08	171.46
17	0.11897	1.174	3.754	4.351	162.08	171.43
18	0.11883	1.179	3.878	4.483	162.09	171.43
19	0.11904	1.175	3.884	4.493	162.08	171.44
20	0.11879	1.180	3.888	4.493	162.13	171.47
21	0.11901	1.179	3.872	4.479	162.06	171.41
22	0.11914	1.180	3.882	4.492	162.05	171.41
23	0.11889	1.169	3.880	4.486	162.12	171.47
24	0.11879	1.178	3.875	4.479	161.86	171.19
25	0.11980	1.169	3.881	4.500	162.97	171.44
26	0.11914	1.182	3.881	4.491	162.12	171.49
27	0.11892	1.171	3.879	4.486	161.89	171.23
28	0.11888	1.176	3.882	4.488	161.88	171.21
29	0.11936	1.176	3.870	4.482	162.34	171.74

TABLE IV: Values of the heavy-quark masses $m_c(m_c)$, $m_b(m_b)$ and $m_t(m_t)$ and $\alpha_s^{(n_f=5)}(M_Z)$ in the $\overline{\text{MS}}$ scheme for the PDFs ABMP16_5_nlo (0+29) with $n_f = 5$. The values for pole masses m_b^{pole} and m_t^{pole} in the on-shell scheme obtained using RunDec [23] are also given.

ABMP16_4_nlo (0+29),
 ABMP16_5_nlo (0+29),

which consist of the central fit (set 0) and additional 29 sets for the combined symmetric uncertainties in all parameters (PDFs, α_s , m_c , m_b and m_t). In each PDF set, the strong coupling α_s is taken in the corresponding scheme, i.e., $\alpha_s^{(n_f=3)}$, $\alpha_s^{(n_f=4)}$ and $\alpha_s^{(n_f=5)}$ which can be related by the standard decoupling relations in QCD. As usual, the PDF set with three light-quarks $n_f = 3$, ABMP16_3_nlo, is valid at all perturbative scales $\mu^2 \gtrsim 1 \text{ GeV}^2$, while those with $n_f = 4$ and $n_f = 5$, ABMP16_4_nlo and ABMP16_5_nlo, are subject to minimal cuts in $\mu^2 \geq 3 \text{ GeV}^2$ and $\mu^2 \geq 20 \text{ GeV}^2$, respectively, cf. Ref. [4] for additional discussions.

For studies of LHC observables and their dependence on α_s we also provide NLO PDF grids for $n_f = 5$ flavors with the central value of $\alpha_s^{(n_f=5)}(M_Z)$ fixed. The 10 sets cover the range $\alpha_s^{(n_f=5)}(M_Z) = 0.114 \div 0.123$ with a spacing of 0.001 and are denoted as

ABMP16als114_5_nlo (0+29),
 ABMP16als115_5_nlo (0+29),
 ABMP16als116_5_nlo (0+29),
 ABMP16als117_5_nlo (0+29),
 ABMP16als118_5_nlo (0+29),
 ABMP16als119_5_nlo (0+29),
 ABMP16als120_5_nlo (0+29),
 ABMP16als121_5_nlo (0+29),
 ABMP16als122_5_nlo (0+29),
 ABMP16als123_5_nlo (0+29),

where the value of $\alpha_s^{(n_f=5)}(M_Z)$ has been fixed as indicated in the file names. These grids are determined by re-fitting all PDF parameters for the individual choices of α_s , which for technical consistency remains a formal parameter in the fit, but with greatly suppressed uncertainty.

As the heavy-quark masses $m_c(m_c)$, $m_b(m_b)$ and $m_t(m_t)$ have been fitted their numerical values vary for each of the 29 PDF sets and cross section computations involving heavy quarks have to account for this. For reference we list in Tab. IV the heavy-quark masses in the ABMP16 grids and the values of $\alpha_s^{(n_f=5)}(M_Z)$. These values can also be easily retrieved within the LHAPDF library framework. The bottom- and the top-quark pole masses, m_b^{pole} and m_t^{pole} , which are required for the on-shell scheme are also provided in Tab. IV. In particular, for computations with the central ABMP16 set at NLO the values $m_b^{\text{pole}} = 4.488 \text{ GeV}$ and $m_t^{\text{pole}} = 171.44 \text{ GeV}$ should be used.²

Finally, we also provide the results of the variants with no constraints on the fit parameters, in particular on the higher-twist terms, which are extracted at NLO as well. For $n_f = 3, 4$ and 5 flavors these are the sets

ABMP16free_3_nlo (0+29),
 ABMP16free_4_nlo (0+29),
 ABMP16free_5_nlo (0+29),

² In the matching of $m_c(m_c)$ to the on-shell scheme m_c^{pole} acquires large QCD corrections up to N³LO [14], therefore use of m_c^{pole} is problematic in this context [1].

	$\sigma(H)$ [pb] at $\sqrt{s} = 13$ TeV	$\sigma(t\bar{t})$ [pb] at $\sqrt{s} = 5$ TeV	$\sigma(t\bar{t})$ [pb] at $\sqrt{s} = 7$ TeV	$\sigma(t\bar{t})$ [pb] at $\sqrt{s} = 8$ TeV	$\sigma(t\bar{t})$ [pb] at $\sqrt{s} = 13$ TeV
NLO, ABMP16_5_nlo	33.59 ± 0.58	63.74 ± 1.44	172.0 ± 3.3	247.9 ± 4.5	835.3 ± 14.3
NNLO, ABMP16_5_nnlo	40.20 ± 0.63	63.66 ± 1.60	171.8 ± 3.4	247.5 ± 4.6	831.4 ± 14.5

TABLE V: Cross sections at NLO and NNLO in QCD for the Higgs boson production from gluon-gluon fusion ($\sigma(H)$ computed in the effective theory) at $\sqrt{s} = 13$ TeV for $m_H = 125.0$ GeV with the renormalization and factorization scales set to $\mu_r = \mu_f = m_H$ and for the top-quark pair production, $\sigma(t\bar{t})$, at various center-of-mass energies of the LHC with the top-quark mass $m_t(m_t)$ in the $\overline{\text{MS}}$ scheme and $\mu_r = \mu_f = m_t(m_t)$. The values of $\alpha_s(M_Z)$ and $m_t(m_t)$ are order dependent, see Eq. (1) and Tab. III. The errors denote the PDF and α_s uncertainties.

which come, as discussed above, essentially with larger values for $\alpha_s(M_Z)$ and $m_t(m_t)$, e.g., $\alpha_s^{(n_f=5)}(M_Z) = 0.1227$ and $m_t(m_t) = 164.47$ GeV.

The benchmark cross sections for the Higgs-boson and top-quark pair production at the LHC at NLO and NNLO with consistent use of the PDF sets obtained in the present analysis are given in Tab. V. The quoted errors denote the PDF and α_s uncertainties derived from the uncertainties in the experimental data. Thus, they are of similar size at NLO and NNLO.

The Higgs boson cross section $\sigma(H)$ is computed in the effective theory in the limit $m_t \rightarrow \infty$, but with full m_t dependence in the Born cross section, based on the NNLO results of Refs. [15–17]. The NLO value of $\sigma(H)$ is about 20% smaller than the NNLO one due to missing large perturbative corrections, which are only partially compensated by a larger value of α_s . In the effective theory the Born cross section for $\sigma(H)$ is proportional to α_s^2 , so that the variant of the NLO fit with the larger value for the strong coupling, $\alpha_s^{\text{NLO}}(M_Z) = 0.1227$, gives a NLO cross section increased by 5%, i.e. $\sigma(H) = 35.2 \pm 0.58$ pb with the PDF set ABMP16free_5_nlo compared to $\sigma(H) = 33.59 \pm 0.58$ pb with the PDF set ABMP16_5_nlo in Tab. V.

The inclusive cross section $\sigma(t\bar{t})$ for top-quark pair production uses Ref. [18] based on Refs. [19–22]. In this case, the NLO and NNLO values of $\sigma(t\bar{t})$ for the range of center-of-mass energies explored at the LHC are similar, since those data have been included in both fits and are accommodated by the corresponding changes in the value of α_s and the top-quark mass m_t , cf. Fig. 3 and Tab. III.

In summary, we have completed the determination of the ABMP16 PDF sets at those orders of perturbation theory, which are currently of phenomenological relevance, i.e., at NLO and NNLO. Essential input in the ABMP16 analysis has been the final HERA DIS combination data from run I+II, which has consolidated the available world DIS data. In addition, several new data sets from the fixed-target DIS together with recent LHC and Tevatron data for the DY process and for the top-quark hadro-production have been used.

We have discussed the features of the NLO extraction of PDFs, which in general, have a few limitations due to lacking constraints of the higher order Wilson coefficients and we have emphasized the consistent use of PDFs and an order-dependent value of $\alpha_s(M_Z)$, which is absolutely crucial because of correlations. The same holds, to a lesser extent, in collider processes also for the values of the heavy-quark masses used.

The ABMP16 PDFs establish the baseline for high precision analyses of LHC data from run I

and run II, and the NLO variant is now available for computing cross sections of scattering processes with multi-particle final states, for which the NNLO QCD corrections will not be available in the foreseeable future, or for Monte Carlo studies. Precision analyses of LHC data, however, will always require analyses to NNLO accuracy in QCD. This will become even more important with the arrival of the data from the high luminosity runs.

Acknowledgments: We would like to thank K. Lipka and O. Zeniaev for cross-checks of the preliminary version of the LHAPDF grids derived from this analysis. This work has been supported by Bundesministerium für Bildung und Forschung (contract 05H15GUCC1).

-
- [1] A. Accardi *et al.*, Eur. Phys. J. **C76**, 471 (2016), arXiv:1603.08906.
 - [2] S. Alekhin, J. Blümlein, and S. Moch, Phys. Rev. **D86**, 054009 (2012), arXiv:1202.2281.
 - [3] S. Alekhin, J. Blümlein, and S. Moch, Phys. Rev. **D89**, 054028 (2014), arXiv:1310.3059.
 - [4] S. Alekhin, J. Blümlein, S. Moch, and R. Placakyte, Phys. Rev. **D96**, 014011 (2017), arXiv:1701.05838.
 - [5] A. Buckley *et al.*, Eur. Phys. J. **C75**, 132 (2015), arXiv:1412.7420.
 - [6] J. Blümlein, S. Riemersma, W. L. van Neerven, and A. Vogt, Nucl. Phys. Proc. Suppl. **51C**, 97 (1996), arXiv:hep-ph/9609217.
 - [7] S. Alekhin, J. Blümlein and S. O. Moch, Mod. Phys. Lett. A **31** (2016) no.25, 1630023.
 - [8] H1 Collaboration, V. Andreev *et al.*, Eur. Phys. J. C **77** (2017) no.11, 791, arXiv:1709.07251.
 - [9] J. Rojo *et al.*, J. Phys. **G42**, 103103 (2015), arXiv:1507.00556.
 - [10] S. Dulat *et al.*, Phys. Rev. **D93**, 033006 (2016), arXiv:1506.07443.
 - [11] NNPDF, R. D. Ball *et al.*, Eur. Phys. J. **C77**, 663 (2017), arXiv:1706.00428.
 - [12] K. Prytz, Phys. Lett. B **311**, 286 (1993).
 - [13] L. A. Harland-Lang, A. D. Martin, P. Motylinski and R. S. Thorne, Eur. Phys. J. C **76** (2016) no.1, 10, arXiv:1510.02332.
 - [14] P. Marquard, A. V. Smirnov, V. A. Smirnov and M. Steinhauser, Phys. Rev. Lett. **114**, 142002 (2015), arXiv:1502.01030.
 - [15] R. V. Harlander and W. B. Kilgore, Phys. Rev. Lett. **88**, 201801 (2002), arXiv:hep-ph/0201206.
 - [16] C. Anastasiou and K. Melnikov, Nucl. Phys. **B646**, 220 (2002), arXiv:hep-ph/0207004.
 - [17] V. Ravindran, J. Smith, and W. L. van Neerven, Nucl. Phys. **B665**, 325 (2003), arXiv:hep-ph/0302135.
 - [18] M. Aliev *et al.*, Comput. Phys. Commun. **182**, 1034 (2011), arXiv:1007.1327.
 - [19] P. Bärnreuther, M. Czakon, and A. Mitov, Phys. Rev. Lett. **109**, 132001 (2012), arXiv:1204.5201.
 - [20] M. Czakon and A. Mitov, JHEP **12**, 054 (2012), arXiv:1207.0236.
 - [21] M. Czakon and A. Mitov, JHEP **01**, 080 (2013), arXiv:1210.6832.
 - [22] M. Czakon, P. Fiedler, and A. Mitov, Phys. Rev. Lett. **110**, 252004 (2013), arXiv:1303.6254.
 - [23] K. G. Chetyrkin, J. H. Kühn, and M. Steinhauser, Comput. Phys. Commun. **133**, 43 (2000), arXiv:hep-ph/0004189.